Journal of Materials Science: Materials in Electronics (2019) 30:6575–6582
https://doi.org/10.1007/s10854-019-00964-3

Electrochemical migration failure mechanism and dendrite composition characteristics of Sn96.5Ag3.0Cu0.5 alloy in thin electrolyte films

Pan Yi[1] · Chaofang Dong[1] · Yucheng Ji[1] · Yupeng Yin[1] · Jizheng Yao[1] · Kui Xiao[1]

Received: 21 January 2019 / Accepted: 16 February 2019 / Published online: 5 March 2019
© Springer Science+Business Media, LLC, part of Springer Nature 2019

Abstract
The effects of chloride ions on electrochemical migration (ECM) of Sn96.5Ag3.0Cu0.5 (SAC 305) solder alloy are studied through in situ electrochemical observation device and ex situ transmission electron microscope (TEM) and X-ray photoelectron spectroscopy (XPS) techniques. The results show that the time to short circuit is the longest at intermediate NaCl concentration, which is related to the precipitates between two electrodes. The composition of dendrite inspected by TEM-EDS and XPS techniques shows that dendrites do not contain elements Ag and Cu, which suggests that Sn is the only migration element in SAC 305 alloy.

1 Introduction

In the electronic packaging industries, the lead bearing solders alloy have already been gradually replaced by lead-free solder paste in recent years due to the Restriction of Hazardous Substance (RoHS) requirement from European Union [1]. Among them, the ternary Sn-Ag-Cu (SAC) alloy is recommended as a promising solder material. Specifically, Sn96.5Ag3.0Cu0.5 alloy (SAC 305) is current best option for the electronics manufacturing results from the low-cost and effectiveness [2–4]. However, it is noteworthy that the reliability and environmental adaptability of the solder alloy are still the enormous challenge in the electronic field. One of these important topics is the electrochemical migration (ECM) failure phenomenon, which can cause the occurrence of catastrophic damages and decrease significantly the service life [5, 6].

In recent decades, a lot of literatures have already reported the ECM phenomenon of Sn-Pb alloy [7–10], copper clad plate [11, 12], pure tin [13, 14], tin solder alloy [15–17] and so on. As a whole, the main test methods related to ECM include water drop (WD) test, thermal humidity bias (THB) test, outdoor exposure test and thin electrolyte film (TEF) test, whose characters and application scope can be refer to literature [11, 18]. For the WD tests, a ring always appears on the water drop surface due to the reflection effects from the light of microscope, which will affect the in situ inspection of dendrite growth. The outdoor exposure test and THB test can well simulate the actual operating conditions of the electronics. However, the shortcoming is poor reproducibility. Compared with these three methods, TEF test has more advantages in in-situ inspection and reproducibility. Thus TEF method receives much more attention in recent years. However, it is noteworthy that almost all the previous experiments concerning the ECM behavior of ternary Sn–Ag–Cu (SAC) alloy were carried out through THB tests and WD tests, while the previous literatures about ECM in the TEF environment mainly focused on the pure Sn materials [13, 14]. To the best of our knowledge, few studies reported the ECM behavior of SAC 305 in TEF environment.

More importantly, almost all the reported TEF methods [13, 14, 19, 20] used a micrometer with a sharp Pt needle and an ohmmeter to measure the electrolyte thickness covered on the sample surface (Fig. S1). As we know, the electrolyte will agglomerate easily at the tip of Pt needle due to the capillary attraction when needle is close to the electrolyte (Fig.

Electronic supplementary material The online version of this article (https://doi.org/10.1007/s10854-019-00964-3) contains supplementary material, which is available to authorized users.

✉ Chaofang Dong
cfdong@ustb.edu.cn

[1] Beijing Advanced Innovation Center for Materials Genome Engineering, Key Laboratory for Corrosion and Protection (MOE), University of Science and Technology Beijing, Beijing 100083, People's Republic of China

S2), which will significantly affect the measurement accuracy of the TEF thickness. Consequently, a TEF device that can effectively avoid capillary action and improve the measurement accuracy is very necessary and important for the study of ECM. On the other hand, concerning the composition of dendrites, the previous studies gave a controversial view [17, 21–23]. For example, Yu et al. [21] and Noh et al. [23] thought that Sn is the only migration element in ternary alloy, and the study from Hua et al. [17] showed that the composition of the dendrite was mainly Cu and Sn, while He et al. [22] suggested that Ag also migrated occasionally beside Sn and Cu. Thus it is very important to further clarify the composition of dendrites for illustrating ECM failure mechanism of the electronic components.

In this paper, an innovative in situ TEF measurement device with high accuracy is designed. Then the effects of chloride ions on the ECM of SAC 305 alloy are in situ investigated through abovementioned device. Moreover, the composition of the dendrite is also further ex situ clarified by transmission electron microscope (TEM) with an energy dispersive spectrometer (EDS) and X-ray photoelectron spectroscopy (XPS) technique.

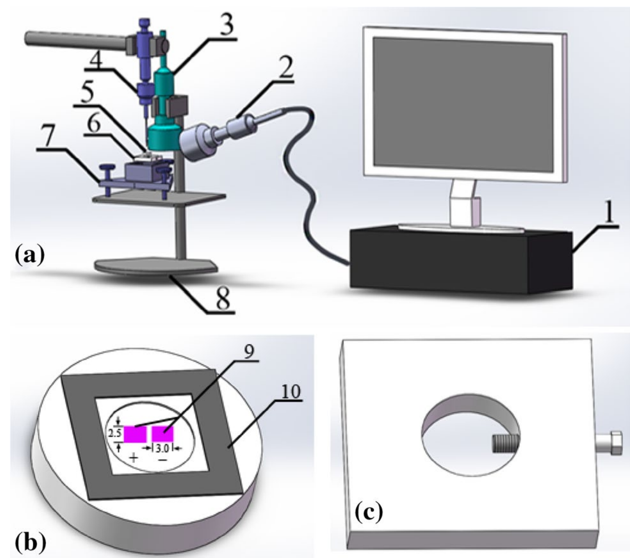

Fig. 1 Schematic diagram of the device for in situ study of electrochemical migration (**a**); the enlarged image of the part 5 (**b**); the enlarged image of the part 6 (**c**): (1) computer; (2) a portable digital microscope for determining the thickness of a liquid film; (3) a stereo microscope (Keyence VHX-2000) for observing the electrochemical migration; (4) A micrometer with tip; (5) sealed samples with epoxy resin; (6) sample hold; (7) height-adjustable test container; (8) a iron stand; (9) samples (SAC 305); (10) filter paper

2 Experimental sections

2.1 Specimens preparation

SAC 305 alloy (Thousand Island Co., China) with the dimensions of $2.5 \times 3.0 \times 8$ mm is used in this work. The chemical composition of the SAC 305 alloy is given in Table 1. Two identical SAC 305 alloy stripes, i.e. anode and cathode respectively, with 0.4 mm spacing in parallel direction are embedded in the epoxy resin. Two copper wires are welded to the backside of electrodes separately. Before each experiment, the samples are polished up to 2000 grit emery paper. Subsequently, the samples are cleaned using ethanol and distilled water, successively and dried by cool air.

2.2 Experimental device design

The innovative TEF measurement device is shown in Fig. 1a. In this paper, a thin electrolyte film with a thickness of 300 μm will be described as an example. The sealed sample with epoxy resin (Fig. 1b) is firstly assembled on the sample hold (Fig. 1c). Then, a filter paper with the corresponding size hole is covered on the holder to ensure that the electrolyte solution spread uniformly on the sample surface. Secondly, a spirit level is placed on the sample surface and adjusts the height-control knob so that the sample is in the horizontal position. Thirdly, open the computer and the portable digital microscope, then focus the microscope on the sample surface. Slowly rotate the micrometer to make the tip just touch the sample surface (Fig. 2a). At this moment, the rotation is suspended immediately and records the indication *A* of the micrometer. Fourthly, rotate the micrometer in the opposite direction so that the distance between the tip and the sample surface is $A + 350$ μm. In other words, the distance between needle tip and its inverted image is 700 μm (Fig. 2b) at that moment. Subsequently, the electrolyte solution is gradually added into the test container. Stop adding solution immediately when the distance between the tip and its inverted image is 100 μm (Fig. 2c). At that time, the distance between the tip and the electrolyte surface is 50 μm, i.e., the thickness of the electrolyte solution is 300 μm. During the whole process, agglomeration phenomenon does not occur. Consequently, the thickness of TEF can be measured accurately.

Table 1 The chemical composition of SAC 305 alloy (wt%)

Alloy	Sn	Ag	Cu	Pb	Sb	Ni	Bi	Fe	In
SAC 305	Bal.	2.968	0.523	0.008	0.011	0.005	0.002	0.004	0.003

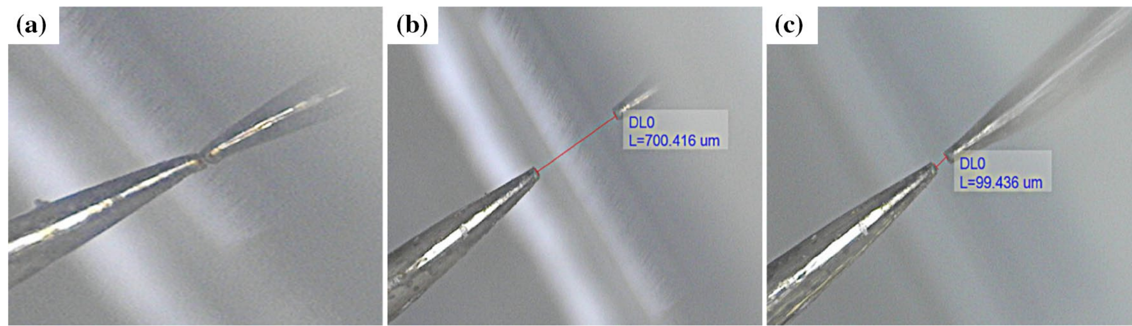

Fig. 2 The test step and method of TEF thickness: **a** the tip just touch the sample surface; **b** the distance between the tip and the sample surface is 350 µm; **c** the distance between the tip and its inverted image is 100 µm

2.3 Electrochemical migration tests

For the ECM experiments, an electrochemical workstation (potentiostatic mode) is used to apply the direct current (DC) bias voltage (3 V) and simultaneously records the relationship curves of current vs. time. The counter electrode and reference electrode of the electrochemical workstation are connected with one of metallic stripes of the sample. The working electrode is connected to another metallic stripe of the sample. The ECM process is in situ observed by the stereo microscope (VHX-2000, Keyence, Japan). The pH distribution on the surface of samples is also in situ inspected using a diluted pH indicator that is prepared by commercial pH indicator (30 ml) and deionized water (100 ml). The electrolyte is various concentrations NaCl solution, which is prepared from analytical grade reagents and deionized water. To ensure the results reproducibility, all the ECM tests are repeated at least five times.

2.4 Topography and composition characterization of the dendrite

After ECM experiments, the micro-topographies of the dendrite are observed by the scanning electron microscope (FEI Quanta 250, America), and the composition of the dendrite is inspected by transmission electron microscope (TEM, FEI TECNAI F20) with an energy dispersive spectrometer (EDS) and X-ray photoelectron spectroscopy (XPS, PHI Quantera II, Japan). The binding energy is adjusted for a charging effect by referencing the C1s peak (284.8 eV). Samples are prepared for TEM-EDS analysis using the focused ion beam (FIB) technique. The obtained TEM samples are welded to the TEM grid made of metal Mo. For the XPS tests, the samples are firstly etched by Ar^+ bombardment for 5 min to remove the effects of the contamination. The etching rate of the sample is 15.3 nm/min relative to SiO_2. The samples for XPS tests are obtained by the cellulose tape.

3 Results and discussion

3.1 Dendrites topographies and the time to short circuit

Figure 3 shows the dendrites topographies and the relationship curves of current density vs. time in 300 µm TEF containing different concentrations of Cl^- with 3 V bias voltage. Under the low NaCl concentration condition, the dendrite is just observed at local area (Fig. 3a, b), while the dendrites almost emerge at whole edge of cathode with the increasing of chloride ion concentration. The SEM magnification diagrams on the upper right corner show that the dendrites are short and slim in low chloride ion concentration. However, for 30 mM and 100 mM solution, the dendrites become much coarser and have longer branches. It is noteworthy that some new side-branches are also formed on the secondary dendrites. When the NaCl concentration exceeds 200 mM, the primary dendrites and the branches show the thin and long appearance. This is mainly due to the poor conductivity of low concentration NaCl solution, which is also indicated by the initial polarization current density (Fig. 3g). In this situation, the anode only slightly corrodes (Fig. 3a), thus the amount of dissolved metal ions is very small. Consequently, the dendrite just nucleates at local cathodic site and then grows toward anode. In addition, the time to short circuit is very long, as is shown in Fig. 3h. However, for 10 mM NaCl solution, the solution conductivity is enhanced and the initial current density increased (Fig. 3g), which also results in the aggravation of anode corrosion occurs (Fig. 3b) and providing more metal cations for the ECM process. Thus the time to short circuit decreases (Fig. 3h). As the concentration of NaCl continually increases, a large amount of metal ions are generated due to the serious anodic dissolution reaction (Fig. 3c–f), which leads to the dendritic nucleation at different sites. Moreover, the dendrites clearly become coarser and longer. Interestingly, the time to short circuit significantly increases for the 30 mM NaCl solution. This phenomenon can be explained as follow: a lot of hydroxyl

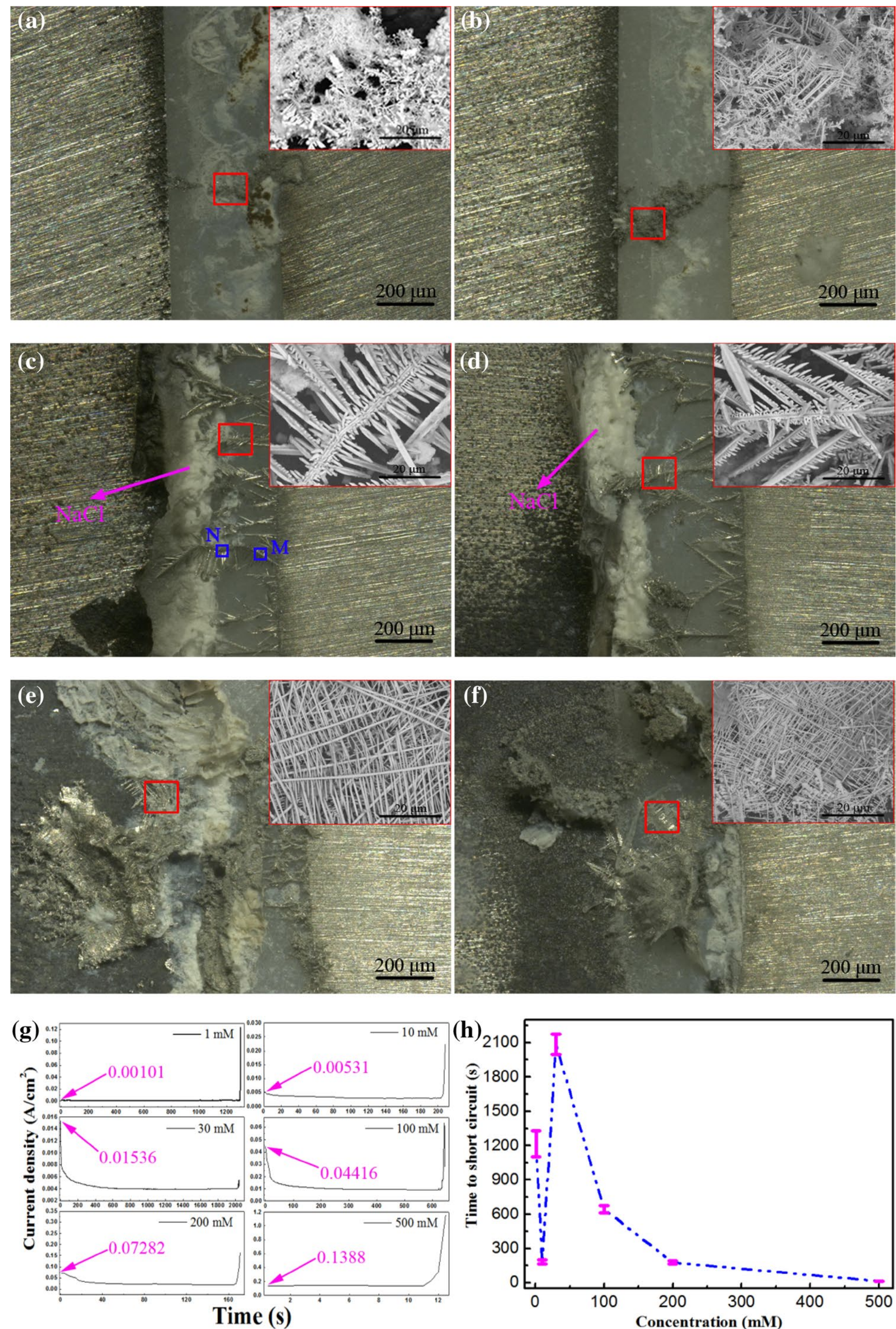

Fig. 3 The dendrites topographies and the relationship curves of current density versus time in 300 μm TEF containing different concentrations of Cl^- with 3 V bias voltage at different time intervals: **a** 1 mM, 1298 s; **b** 10 mM, 205 s; **c** 30 mM, 2025 s; **d** 100 mM, 613 s; **e** 200 mM, 168 s; **f** 500 mM, 12 s; **g** the relationship curves of current density versus time; **h** the average failure time; (anode is on the left and cathode is on the right)

ions are produced at cathode due to the violent hydrogen evolution reaction, which can be confirmed by the pH value mapping, as is shown in Fig. S3. These hydroxyl ions continuously migrate to anode and meet with metal ions, which results in the accumulation of hydroxide or oxide precipitates between two metallic strips. On the other hand, severe hydrogen evolution leads to the saturation of electrolyte near the cathode and causes the precipitation of NaCl (Fig. 3c). Due to the strong disturbance from the large amounts of hydrogen bubbles, the NaCl precipitates also accumulate between the electrodes. Consequently, these precipitates, like a wall, will hinder the migration process of metal ions and lengthen the ECM failure time. Moreover, the previous work also reported that the growth rate of single dendrite might decrease due to the increasing of nucleation sites [13]. For much higher NaCl concentration, more hydroxide ions

will be produced at cathode, which will cause the initial hydroxide or oxide precipitations to dissolve and further migrate to cathode [13]. On the other hand, the stronger disturbance from the hydrogen evolution has much greater driving force and will also push the NaCl precipitates toward the anode instead of accumulating between the two electrodes, which will weaken the barrier effects of the precipitates. Thus the time to short circuit gradually decreases when the NaCl concentration ranges from 30 to 500 mM.

For the intermediate concentration NaCl solution (30 mM and 100 mM), the primary dendrites can not grow smoothly toward anode due to the impediment of precipitates. In this case, a lot of metal ions distribute between the electrodes due to the serious anode dissolution reaction. Consequently these metal ions will nucleate and grow on the secondary dendrites and form more side-branches (Fig. 3c, d). For the higher concentration NaCl solution, a great number of metal ions and severe hydrogen evolution lead to the rapid nucleation and growth of dendrites. The barrier effects from the precipitates almost disappear. Thus the dendrites show thin and long appearance.

3.2 The composition of dendrite

In this paper, the transmission electron microscope with an energy dispersive spectrometer is used to observe the composition of the dendrite, as is shown in Fig. 4. The dendrites in Fig. 4a, d are prepared through FIB technique from area M and area N in Fig. 3c, respectively. Figure 4b, c are the EDS result and selected area electron diffraction (SAED) pattern of the dendrite in Fig. 4a. Figure 4e is the EDS result corresponding to the dendrite in Fig. 4d. The EDS results of dendrites show that there is presence of metallic element Sn and Mo in the dendrite. The element Mo is attributed

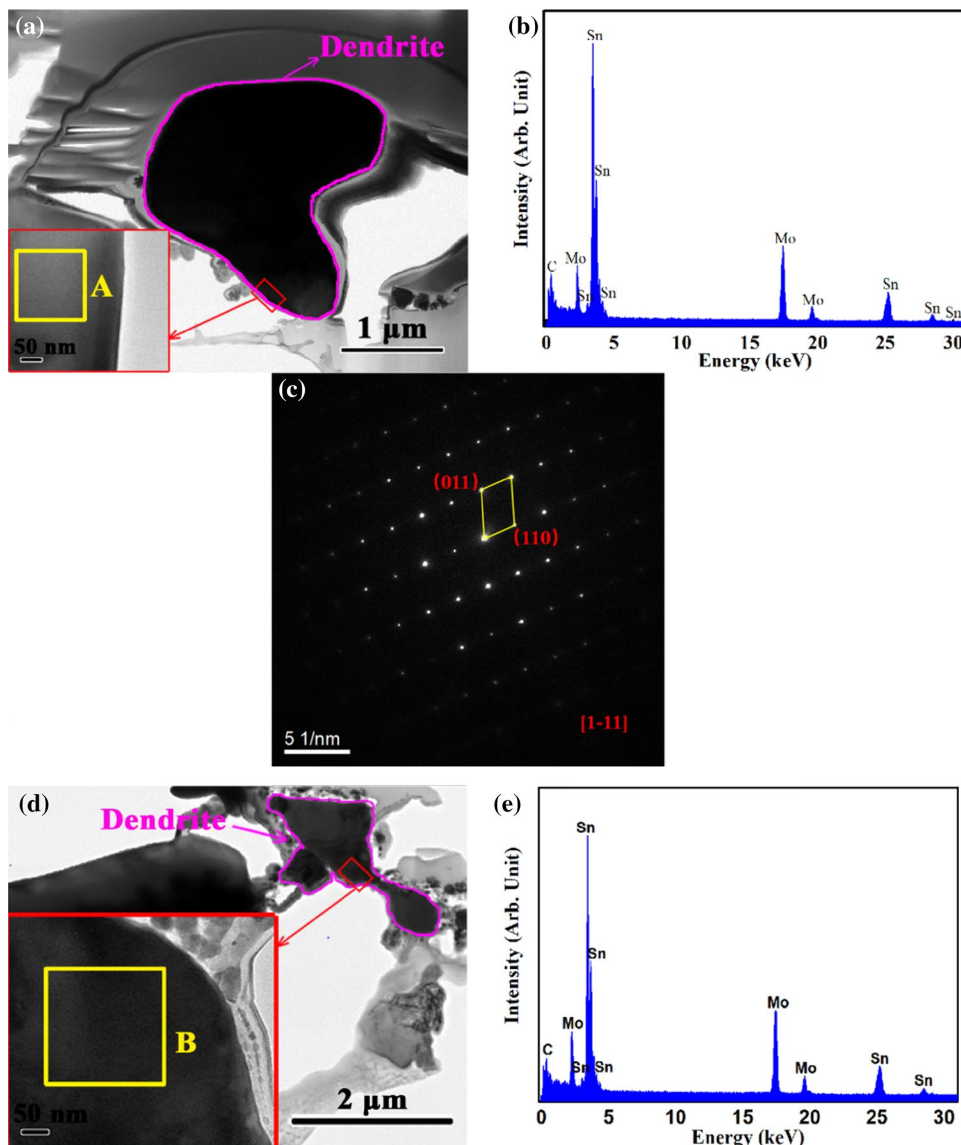

Fig. 4 TEM-EDS and selected area electron diffraction (SAED) pattern test results of the dendrite formed in 30 mM NaCl TEF environment; the dendrite in (**a**) is from area M in Fig. 3c, **b**, **c** is the corresponding EDS and SAED result of dendrite in (**a**); the dendrite in (**d**) is from area N in Fig. 3c, **e** is the corresponding EDS result of dendrite in (**d**); the pictures in the lower left corner in (**a**) and (**d**) are the corresponding high magnification pictures

to the TEM grid. Consequently, it can be concluded that the dendrite do not contain elements Ag and Cu. Moreover, the dendrites located in different area (M and N) show the same result. In order to further confirm the conclusion of the TEM-EDS, selected electron diffraction method is also applied. Figure 4c shows that the dendrite structure is monocrystalline. This SAED pattern can be indexed to the (011) and (110) lattice plans from the zone axis [1–11], which corresponds to a tetragonal structure Sn. As a whole, EDS and SAED pattern result signify that only element Sn undergo the ECM process. Although element Ag and Cu are very susceptible to ECM [24, 25], these elements tend to form intermetallic compounds with Sn, which will increase the ECM resistance [26–28].

In order to further determine the valence state of Sn in the dendrite, XPS tests are conducted. The XPS data is fitted by XPSPEAK 4.0 software, as is shown in Fig. 4. It can be observed from XPS survey spectrum (Fig. 4a) that the dendrite contains elements Sn, C and O. There is absence of Ag and Cu in the dendrite, which is consistent with the TEM-EDS results. For the TEF containing 1 mM NaCl, the XPS high-resolution spectra (Fig. 5b) of Sn 3d5 is deconvoluted into four peaks at 484.9 eV, 485.1 eV, 486.5 eV and 487.6 eV. The peaks at 484.9 eV and 485.1 eV are attributed to Sn [29, 30]; and the peaks detected at 486.5 eV and 487.6 eV correspond to SnO and SnO_2, respectively [29, 31]. The XPS fitted results (Fig. 5c, d) of the dendrites formed at TEF containing 100 mM and 500 mM NaCl show that there are also existence of SnO and SnO_2 in the dendrite [29–33]. These results fully confirm that Sn is the only migration element in SAC 305 alloy and the dendrite is composed of metallic Sn, SnO and SnO_2. Figure 6 displays the proportion of metallic Sn in the dendrite, which is obtained through the integrated the corresponding peak area. It shows that the amount of Sn gradually decreases with the increasing of NaCl concentration. In other words, the dendrite formed at high NaCl concentration includes a greater amount of tin oxides. This is mainly because the electrochemical reactions are more intense (Fig. 3g) in the case of a higher concentration of NaCl environment, which causes much greater amount metallic ions and hydroxide ions (Fig. S3)

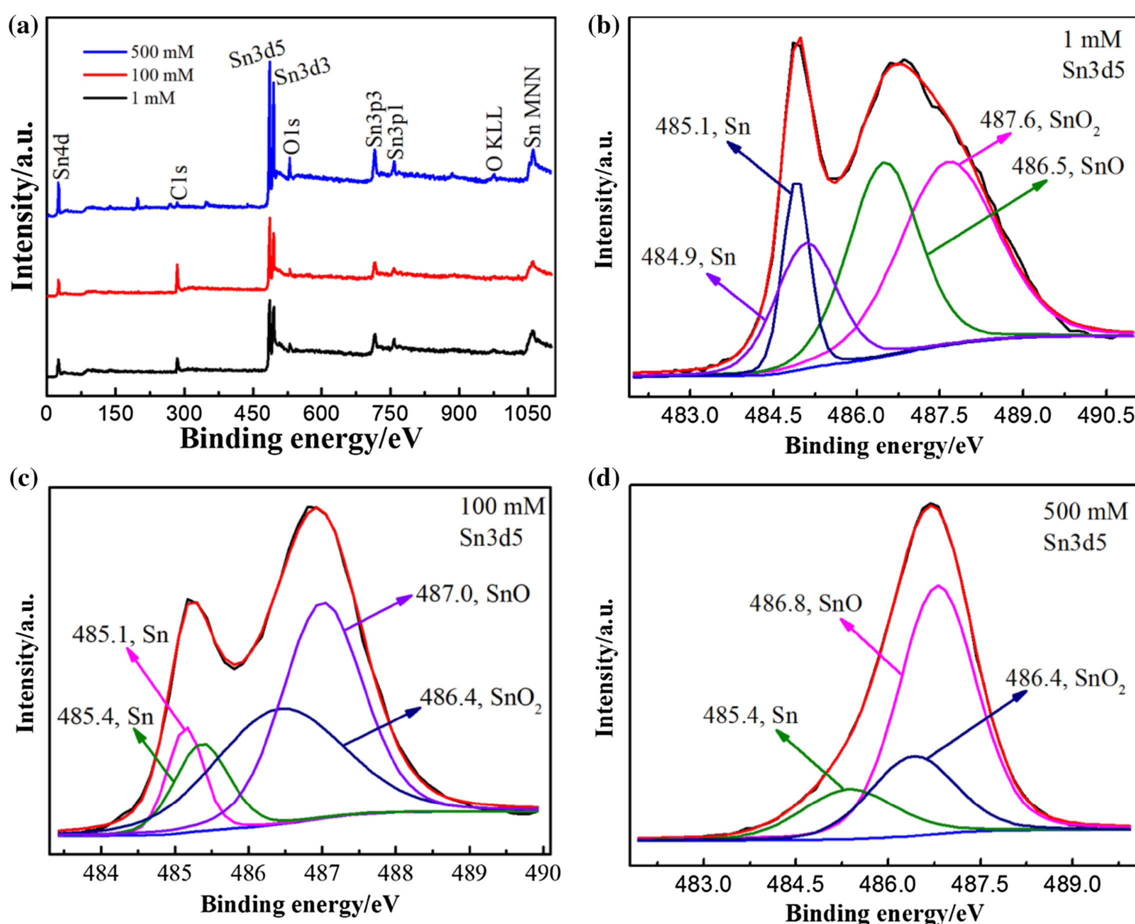

Fig. 5 XPS test results of the dendrites formed at TEF containing different concentration NaCl: **a** XPS survey spectrum; **b–d** XPS high-resolution spectra of Sn3*d*5/2

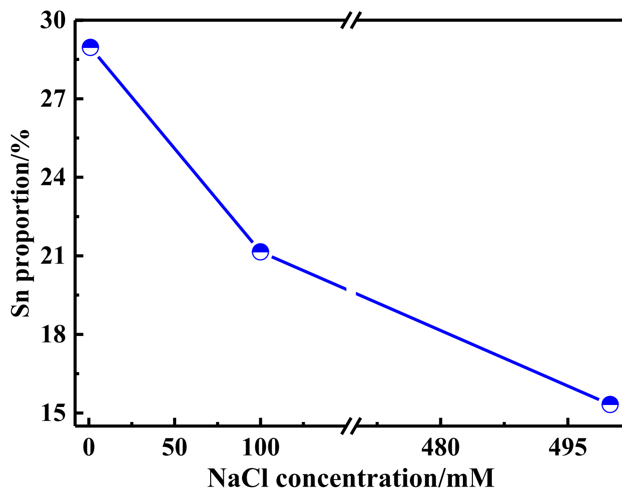

Fig. 6 The relationship curve of Sn proportion in dendrite versus NaCl concentration

between the two metallic stripes. In this situation, a lot of tin oxides are produced when the hydroxide ions encounter with the metallic ions, as is shown in Fig. 3.

3.3 ECM failure mechanism

The concentration of the chloride ions has a significant impact on ECM process. As a whole, the corrosion extent of anode aggravates with the increasing of the concentration of chloride ions. However, the ECM failure time shows different law, which is related to the dendrite topography and the precipitates. Under the intermediate concentration chloride ions condition, the dendrite almost nucleates at whole edge of the cathode, as is shown in Fig. 3c, d, which will decrease the growth rate of the single dendrite. On the other hand, some precipitates accumulated between the two electrodes restraint the migration process of the metallic ions and hydroxide ions. In this situation, some secondary dendrites and more branches gradually form along the main dendrite, which also lengthens the short circuit time. Consequently, the short circuit time under intermediate concentration chloride ions condition is the longest. For the much higher concentration chloride ions environment, the greater driving force from the stronger hydrogen evolution will also push the precipitates toward the anode instead of accumulating between the two electrodes, which will weaken the barrier effects of the precipitates. Thus the short circuit time decreases for the higher concentration of chloride ions condition. Moreover, it is noteworthy that TEM-EDS and XPS results clearly confirm that the element Ag and Cu do not undergo the ECM process, which may be attributed to the formation of intermetallic compound with Sn.

4 Conclusions

The effects of chloride ions on the ECM of SAC 305 alloy are studied through self-designed in situ electrochemical observation device. The composition of the dendrite is also further clarified by ex situ TEM-EDS and XPS techniques. The main conclusions obtained from this work are presented as follows:

1. The time to short circuit is the longest at the intermediate NaCl concentration (30 mM), which is related to the accumulation of precipitates between two metallic strips. When the NaCl concentration ranges from 30 to 500 mM, the time to short circuit gradually decreases due to more hydroxide ions and the stronger disturbance from the hydrogen evolution.
2. In low chloride ion concentration, the dendrites are short and slim, while they gradually become coarser and longer and even show more side-branches on the secondary dendrites with the increasing of chloride ions concentration. For the 200 mM and 500 mM NaCl TEF condition, primary dendrites and the branches show the thin and long appearance.
3. For SAC 305 alloy, Ag and Cu do not undergo the ECM process and Sn is the only migration element in this experiment condition. The dendrite is composed of Sn with a tetragonal structure and its oxide. In addition, the amount of tin oxide in the dendrite gradually increased with the increasing of chloride ions concentration.

Acknowledgements This work was supported by the National High Technology Research and Development Program of China (2017YFB0702300); National Natural Science Foundation of China (No. 51671029); and the National Environmental Corrosion Platform (NECP).

References

1. B. Medgyes, B. Horváth, B. Illés, T. Shinohara, A. Tahara, G. Harsányi, O. Krammer, Microstructure and elemental composition of electrochemically formed dendrites on lead-free micro-alloyed low Ag solder alloys used in electronics. Corros. Sci. **92**, 43–47 (2015)
2. S. Chellvarajoo, M. Abdullah, Microstructure and mechanical properties of Pb-free Sn–3.0 Ag–0.5 Cu solder pastes added with NiO nanoparticles after reflow soldering process. Materials & Design **90**, 499–507 (2016)
3. M. Yang, H. Ji, S. Wang, Y.-H. Ko, C.-W. Lee, J. Wu, M. Li, Effects of Ag content on the interfacial reactions between liquid Sn–Ag–Cu solders and Cu substrates during soldering. J. Alloy. Compd. **679**, 18–25 (2016)
4. S. Cheng, C.-M. Huang, M. Pecht, A review of lead-free solders for electronics applications. Microelectron. Reliab. **75**, 77–95 (2017)

5. P. Yi, K. Xiao, K. Ding, C. Dong, X. Li, Electrochemical migration behavior of copper-clad laminate and electroless nickel/immersion gold printed circuit boards under thin electrolyte layers. Materials **10**, 137 (2017)
6. P. Yi, K. Xiao, C. Dong, S. Zou, X. Li, Effects of mould on electrochemical migration behaviour of immersion silver finished printed circuit board. Bioelectrochemistry **119**, 203–210 (2018)
7. D. Yu, W. Jillek, E. Schmitt, Electrochemical migration of Sn-–Pb and lead free solder alloys under distilled water. J. Mater. Sci. **17**, 219–227 (2006)
8. S.B. Lee, Y.R. Yoo, J.Y. Jung, Y.B. Park, Y.S. Kim, Y.C. Joo, Electrochemical migration characteristics of eutectic SnPb solder alloy in printed circuit board. Thin Solid Films **504**, 294–297 (2006)
9. J.Y. Jung, S.B. Lee, H.Y. Lee, Y.C. Joo, Y.B. Park, Electrochemical migration characteristics of eutectic Sn-Pb solder alloy in NaCl and Na_2SO_4 solutions. J. Electron. Mater. **38**, 691–699 (2009)
10. D. Minzari, F.B. Grumsen, M.S. Jellesen, P. Møller, R. Ambat, Electrochemical migration of tin in electronics and microstructure of the dendrites. Corros. Sci. **53**, 1659–1669 (2011)
11. P. Yi, C. Dong, K. Xiao, X. Li, Surface failure analysis of a field-exposed copper-clad plate in a marine environment with industrial pollution. Appl. Surf. Sci. **399**, 608–616 (2017)
12. P. Yi, K. Xiao, K. Ding, L. Yan, C. Dong, X. Li, Initial corrosion behavior of a copper-clad plate in typical outdoor atmospheric environments. Electron. Mater. Lett. **12**, 163–170 (2016)
13. X. Zhong, G. Zhang, Y. Qiu, Z. Chen, X. Guo, Electrochemical migration of tin in thin electrolyte layer containing chloride ions. Corros. Sci. **74**, 71–82 (2013)
14. X. Zhong, G. Zhang, Y. Qiu, Z. Chen, W. Zou, X. Guo, In situ study the dependence of electrochemical migration of tin on chloride. Electrochem. Commun. **27**, 63–68 (2013)
15. Y. Xia, W. Jillek, E. Schmitt, In-situ observation on electrochemical migration of lead-free solder joints under water drop test, in Electronic Packaging Technology & High Density Packaging, 2008. ICEPT-HDP 2008. International Conference on, IEEE, pp. 1–5 (2008)
16. B. Medgyes, D. Rigler, B. Illés, G. Harsányi, L. Gál, Investigating of electrochemical migration on low-ag lead-free solder alloys, in: Design and Technology in Electronic Packaging (SIITME), 2012 IEEE 18th International Symposium for, IEEE, pp. 147–150 (2012)
17. L. Hua, C. Yang, Corrosion behavior, whisker growth, and electrochemical migration of Sn–3.0 Ag–0.5 Cu solder doping with In and Zn in NaCl solution. Microelectron. Reliab. **51**, 2274–2283 (2011)
18. X. Zhong, S. Yu, L. Chen, J. Hu, Z. Zhang, Test methods for electrochemical migration: a review. J. Mater. Sci.: Mater. Electron. **28**, 2279–2289 (2017)
19. G.Q. Lu, C. Yan, Y. Mei, X. Li, Dependence of electrochemical migration of sintered nanosilver on chloride. Mater. Chem. Phys. **151**, 18–21 (2015)
20. B. Liao, Z. Chen, Y. Qiu, G. Zhang, X. Guo, Effect of citrate ions on the electrochemical migration of tin in thin electrolyte layer containing chloride ions. Corros. Sci. **112**, 393–401 (2016)
21. D. Yu, W. Jillek, E. Schmitt, Electrochemical migration of lead free solder joints. J. Mater. Sci. **17**, 229–241 (2006)
22. X. He, M.H. Azarian, M.G. Pecht, Evaluation of electrochemical migration on printed circuit boards with lead-free and tin-lead solder. J. Electron. Mater. **40**, 1921–1936 (2011)
23. B.I. Noh, S.-B. Jung, Behaviour of electrochemical migration with solder alloys on printed circuit boards (PCBs). Circuit World **34**, 8–13 (2008)
24. B. Medgyes, B. Illés, G. Harsányi, Electrochemical migration behaviour of Cu, Sn, Ag and Sn63/Pb37. J. Mater. Sci. **23**, 551–556 (2012)
25. B.I. Noh, J.B. Lee, S.B. Jung, Effect of surface finish material on printed circuit board for electrochemical migration. Microelectron. Reliab. **48**, 652–656 (2008)
26. N.K. Othman, K.Y. Teng, A. Jalar, F.C. Ani, Z. Samsudin, Electrochemical migration behaviours of low silver content solder alloy SAC 0307 on printed circuit boards (PCBs) in NaCl solution, in: Materials Science Forum (2016)
27. Y.R. Yoo, H. Nam, Y.S. Kim, S.B. Lee, J. Jung, Y.B. Park, Y. Joo, Influence of corrosion properties on electrochemical migration of Sn, SnAg, SnAgCu solder alloys, in: Meeting Abstracts, The Electrochemical Society, pp. 826–826 (2007)
28. M.C. Liew, I. Ahmad, L.M. Lee, M.F.M. Nazeri, H. Haliman, A.A. Mohamad, Corrosion behavior of Sn-3.0 Ag-0.5 Cu lead-free solder in potassium hydroxide electrolyte. Metall. Mater. Trans. A **43**, 3742–3747 (2012)
29. M. Wang, J. Wang, H. Feng, W. Ke, Effect of Ag3Sn intermetallic compounds on corrosion of Sn-3.0 Ag-0.5 Cu solder under high-temperature and high-humidity condition. Corros. Sci. **63**, 20–28 (2012)
30. R.B. Shalvoy, G. Fisher, P. Stiles, Bond ionicity and structural stability of some average-valence-five materials studied by X-ray photoemission. Phys. Rev. B **15**, 1680 (1977)
31. C. Qin, J. Oak, N. Ohtsu, K. Asami, A. Inoue, XPS study on the surface films of a newly designed Ni-free Ti-based bulk metallic glass. Acta Mater. **55**, 2057–2063 (2007)
32. N. Mora, E. Cano, J. Polo, J. Puente, J. Bastidas, Corrosion protection properties of cerium layers formed on tinplate, Corros. Sci. **46**, 563–578 (2004)
33. W.E. Morgan, J.R. Van Wazer, Binding energy shifts in the X-ray photoelectron spectra of a series of related Group IVa compounds. J. Phys. Chem. **77**, 964–969 (1973)

Publisher's Note Springer Nature remains neutral with regard to jurisdictional claims in published maps and institutional affiliations.